Search for Associated Higgs Boson Production
$VH \rightarrow e^{\pm}\nu_e\mu^{\pm}\nu_\mu$ with Like Charged Electron Muon pairs using 9.7 fb^{-1} of $p\bar{p}$ Collisions at $\sqrt{s} = 1.96$ TeV

The DØ Collaboration
URL http://www-d0.fnal.gov
(Dated: March 5, 2012)

A search for the standard model (SM) Higgs boson associated production is presented using a sample of like charge electron and muon events in $p\bar{p}$ collisions at a center-of-mass energy of $\sqrt{s} = 1.96$ TeV. The data, corresponding to an integrated luminosity of 9.7 fb^{-1}, were collected from April 2002 to September 2011 using the DØ detector at Fermilab. No excess above the SM background has been observed and limits on the Higgs boson production cross section times the SM branching ratio for $m_H = 115, 120, \ldots, 200$ GeV are extracted.

Preliminary Result for the Moriond 2012 Conference

I. INTRODUCTION

In the standard model (SM) the masses of the fermions are generated by their interaction with a scalar field, the Higgs boson, which has yet to be discovered. The Higgs boson is the residual degree of freedom after the spontaneous symmetry breaking of the electroweak gauge symmetry $SU(2) \otimes U(1)$ which is responsible for the generation of the masses of the W and Z bosons.

This note describes the search for the associated vector boson production ($p\bar{p} \to VH, V = W, Z$) where the final state has one electron and one muon with the same electric charge. This like charge signature arises mainly in events where the associated Higgs boson decays leptonically and the vector boson decays to a final state involving one or more leptons. The analysis uses data collected with the DØ detector at the Fermilab Tevatron totalling an integrated luminosity of 9.7 fb^{-1}.

One of the primary Higgs boson decay is $H \to WW^*$, which is the dominant decay mode for Higgs boson mass $m_H > 135$ GeV. One obvious advantage of the presence of two like charged leptons is the clear suppression of standard model backgrounds (Z/γ^*, WW, and $t\bar{t}$, etc.). The previous publication used 5.4 fb^{-1} of data collected from DØ [1].

The main irreducible physics backgrounds are $WZ \to l\nu l'l'$, and $ZZ \to lll'l'$ although the latter one has much lower production rate. In addition to the irreducible physics backgrounds, there are also instrumental backgrounds of $e^{\pm}\mu^{\pm}$pairs from multijet or W+jet/γ production.

A two step multivariate analysis based on boosted decision trees (BDT) has been set up. In the first BDT training, the signal is separated from the instrumental backgrounds. The second BDT training discriminates between the signal and the remaining backgrounds. The output of the second BDT training is the final discriminant used to setup a limit for the associated Higgs boson production.

II. DØ DETECTOR

This analysis relies upon the efficient identification of muons, electrons, jets and missing transverse energy using many subsystems of the DØ Run II detector [2]. The central tracking system consists of a silicon microstrip tracker (SMT) and a central fiber tracker (CFT), both located within a 2 T axial magnetic field. The SMT strips have a typical pitch of 50–80 μm, and the design is optimized for tracking and vertexing over the pseudorapidity range $|\eta| < 4.2$, where $\eta = -\ln(\tan\theta/2)$ with θ being the polar angle relative to the proton beam direction. The system has a six-barrel longitudinal structure, with each barrel having a set of four silicon layers arranged axially around the beam pipe. The CFT has eight thin coaxial barrels, each supporting two doublets of overlapping scintillating fibers of 0.835 mm diameter, one doublet parallel to the beam axis, the other alternating by $\pm 3°$ relative to the beam axis.

A set of three liquid-argon/uranium calorimeters surrounds the central tracking system. It consists of a central calorimeter (CC) covering to $|\eta| \approx 1.1$, and two end calorimeters (EC) extending coverage for $|\eta| < 4.2$, each housed in separate cryostats. Scintillators between the CC and EC cryostats provide sampling of showers for $1.1 < |\eta| < 1.4$.

The muon system is located outside the calorimeters and consists of a layer of tracking detectors and scintillation trigger counters inside toroid magnets which provide a 1.8 T magnetic field, followed by two similar layers behind each toroid. Tracking in the muon system for $|\eta| < 1$ relies on 10 cm wide drift tubes, while 1 cm mini-drift tubes are used for $1 < |\eta| < 2$. The numbers of hits in the wire chambers and in the scintillators of the muon spectrometer are combined to define a muon quality variable, used in the final stage of the analysis.

Trigger and data acquisition systems are designed to accommodate the high luminosities of Run II. Based on preliminary information from tracking, calorimetry, and muon systems, the output of the first level of the trigger is used to limit the rate for accepted events to ≈ 1.5 kHz. At the next trigger stage, with more refined information, the rate is reduced further to ≈ 0.8 kHz. These first two levels of triggering rely mainly on hardware and firmware. The third and final level of the trigger, with access to all the event information, uses software algorithms and a computing farm, and reduces the output rate to ≈ 100 Hz, which is written to tape.

The DØ detector was upgraded between February and June of 2006. An new Layer 0 within the SMT [3] is added and a new set of level 1 calorimeter trigger is used [4].

III. DATA AND MONTE CARLO SAMPLES

The data sample used in this analysis was collected between April 2002 and September 2011 (Run II) by the DØ detector at the Fermilab Tevatron collider at $\sqrt{s} = 1.96$ TeV, and corresponds to an integrated luminosity of 9.7 fb^{-1} after imposing data quality requirements. The luminosity is measured using plastic scintillator arrays located in front of the EC cryostats at DØ, covering $2.7 < |\eta| < 4.4$. An overall MC normalization factor ($f_{normalization}$) is obtained from the opposite sign $e\mu$ region in the mass window 35-70 GeV, where the Z+jet events dominate. This

normalization factor of $f_{normalization} = 0.99$, which also confirms the luminosity measurement, is applied to all MC samples.

All signal events are generated using the PYTHIA event generator [5]. The main production channels are WH and ZH. The signal is given by associated production of a Higgs boson, $p\bar{p} \rightarrow VH \rightarrow l^{\pm}l^{\pm}$, which has additional final state particles. Higgs boson decays $H \rightarrow b\bar{b}$ and $H \rightarrow c\bar{c}$ are excluded. All other production channels have negligible yields. The signal cross sections have been calculated for different Higgs boson masses at approximate NNLO and branching ratios as listed in [6]. The individual branching fraction from PYTHIA for the Higgs boson decay channels are normalised to match the precise predictions based on HDECAY program [7].

The main background processes for the analysis are $Z(+\text{jets}) \rightarrow e^+e^-, \mu^+\mu^-, \tau^+\tau^-$, diboson ($p\bar{p} \rightarrow WZ \rightarrow l\nu l'l'$, $p\bar{p} \rightarrow ZZ \rightarrow lll'l'$), W+jet/γ production, the $t\bar{t}$ and multijet. Non-resonant triple vector boson production($VVV, V = W, Z$) is negligibly small. For the simulation of W+jets and Z+jets backgrounds we use the ALPGEN [8] event generator. The background MC samples for inclusive W and Z boson production are normalized using the NNLO cross sections calculations [9] and the NLO CTEQ 6.1 PDF [10]. The Z boson p_T distribution is modelled to match the distribution observed in data [11], taking also into account the dependence on the number of reconstructed jets. The p_T distribution of the W boson is based on the measurement of the Z boson p_T spectrum [11], taking into account the ratio between the W and Z boson p_T distributions at NLO [12]. The production of W bosons contributes to the dilepton background when there is a misidentified lepton, which can originate from a jet or from a photon converting to a pair of electrons. The contribution from these backgrounds are estimated using MC simulations and the data is used to derive corrections to the contributions of jets and photons misidentified as electrons. A W+jet/γ dominated sample orthogonal to the signal region is selected using events passing all the selection criteria but with the charge and electron likelihood requirements reversed. Corrections are obtained separately for Initial State Radiation jets and photons (ISR j/γ) and Final State Radiation photons (FSR γ) by splitting this control sample in high dilepton invariant mass ($M_{ll} > 40$ GeV) and low di-lepton invariant mass ($M_{ll} < 20$ GeV) where the contributions of ISR j/γ and FSR γ, respectively, are dominant. The $t\bar{t}$ cross section is calculated at NNLO [13]. The WW, ZZ and WZ cross sections are calculated in [14, 15] with MCFM using CTEQ6.1M PDFs. The two largest instrumental backgrounds, charge mismeasurement and lepton misidentification, are estimated from data, details can be found in [1]. The charge flip background, created by mismeasurement of the charge of one of the leptons, mostly originates from the Drell-Yan process. This occurs when the curvature of a high p_T track is not correctly measured, or when additional hits from other charged particles and noise are present near the track. The contribution of charge flips to the $e\mu$ selection is very small as the dominant Drell-Yan production must decay via a τ lepton pair and is suppressed by the branching fraction of the τ lepton into an electron or a muon. In addition, leptons from τ decays have a lower p_T spectrum, hence the average charge flip rate is smaller. In the case of jets misidentified as muons, the multijet background contains muons from semileptonic decays of heavy flavor quarks, punch-through hadrons in the muon detector, and muons from pion or kaon decays in flight. In the case of jets misidentified as electrons, the multijet background contains electrons from semileptonic heavy flavor decays, from hadrons misidentified as electrons, and from photon conversions. The multijet background contribution is estimated directly from the data by measuring the ratio of the probability that a jet satisfies the "regular" electron(muon) identification criteria (see Sec. IV) over the probability that a jet satisfies the "reverse" electron(muon) identification criteria as a function of the reconstructed electron(muon) p_T. The product of these ratios are then used as event weights on a pure multijet sample containing a reconstructed electron and muon satisfying the reverse electron and muon identification criteria.

IV. PRESELECTION

All events satisfying any trigger of the DØ trigger suite are accepted for this analysis. While most events selected in the analysis are triggered by single-lepton and dilepton triggers, additional acceptance is gained by including triggers with jets or missing transverse energy. The simulated background samples are normalized to the integrated luminosity and cross section.

Electrons are identified using calorimeter and tracking information. Electromagnetic showers are identified in the calorimeter by comparing the longitudinal and transverse shower profiles to those of simulated electrons. The showers must be isolated, deposit 90% of their energy in the electromagnetic part of the calorimeter and pass a likelihood criterion that includes a spatial track match and, in the central detector region, an E/p requirement, where E is the energy of the calorimeter cluster and p is the momentum of the track. The value of the likelihood variable is referred to as the electron quality. Electrons are required to be in the calorimeter region $|\eta| < 1.1$ or $1.5 < |\eta| < 2.5$. The transverse momentum measurement of the electrons is based on calorimeter energy information.

Muon tracks are reconstructed from hits in the wire chambers and scintillators in the muon system, and must match a track in the central tracker. To select isolated muons, its track transverse momentum isolation ($iso^{\mu}_{trk\_p_T}$) and its transverse energy isolation ($iso^{\mu}_{E_T}$) have to satisfy $iso^{\mu}_{trk\_p_T} < 0.15 \times p^{\mu}_T$, $iso^{\mu}_{E_T} < 0.15 \times p^{\mu}_T$. In addition, the

calorimeter isolation for each muon (Cal_{iso}^{μ}) is required to be $Cal_{iso}^{\mu} < 10$ GeV. Muons are restricted to the fiducial coverage of the muon system $|\eta| < 2.0$. Muons from cosmic rays are rejected by requiring a timing criterion on the hits in the scintillator layers as well as applying restrictions on the position of the muon track with respect to the selected $p\bar{p}$ interaction vertex (PV).

Events with more than one electron or more than one muon satisfying the above selection criteria are excluded from this analysis to avoid overlap when combining with other final states.

Hadronic jets are reconstructed from energy deposits in the calorimeter towers using an iterative midpoint cone algorithm with a cone radius of 0.5 [16]. All calorimeter jets are required to pass a set of quality criteria which are approximately 98% efficient and have at least two reconstructed tracks within $\Delta R(\text{track, jet-axis}) = \sqrt{(\Delta\eta)^2 + (\Delta\phi)^2} \leq 0.5$. Jets are also required to be consistent with originating from the $p\bar{p}$ PV.

The missing transverse energy, $\not{E}_T$, is obtained from a vector sum of transverse components of calorimeter energy depositions and corrected for identified muons. The jet energies are calibrated using transverse momentum balance in photon+jet events and the correction is propagated to the $\not{E}_T$.

We select events where there is one electron with $p_T >15$ GeV, and one muon with 10 GeV$< p_T <$250 GeV and they originate from the same position (within 1 cm) along the beamline. Any additional reconstructed lepton is not considered. In addition, the dilepton invariant mass is required to exceed 15 GeV. This stage of the analysis is referred to as "preselection". Figure 1 shows several kinematic distributions of this channel at preselection. The transverse mass is defined as $M_T = \sqrt{2 \cdot p_T^{\ell} \cdot \not{E}_T \cdot (1 - \cos\Delta\phi(\ell, \not{E}_T))}$ and the minumum transverse mass is $M_T^{\min} = \min(M_T^{\ell_1}, M_T^{\ell_2})$.

The number of events at preselection are shown in Table I. In general, good agreement between data and the expected background contribution is observed. At this stage, the W+jet/γ contribution and multi-jet events are the dominant background sources.
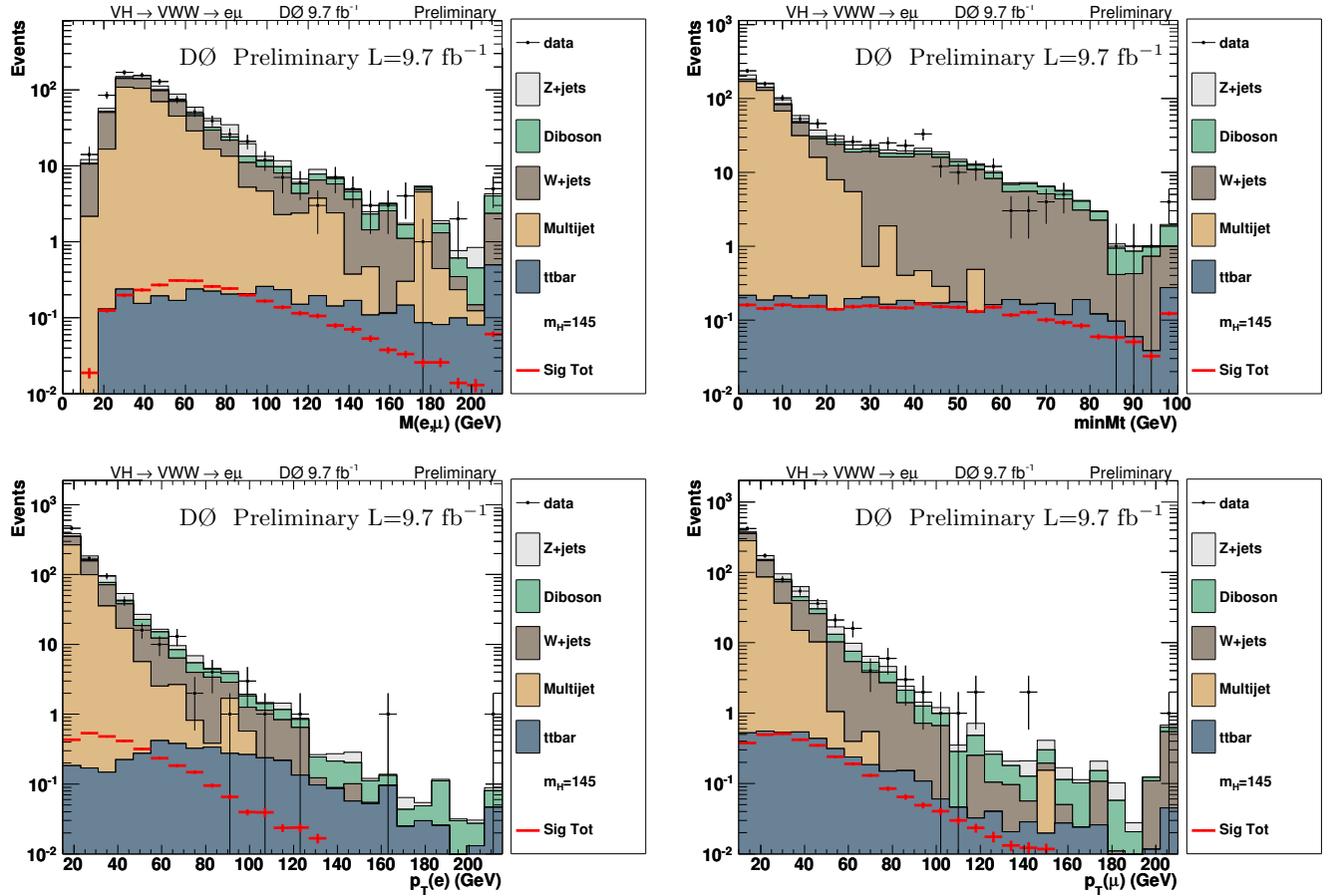

FIG. 1: The invariant mass(M(e,μ)), minimum transverse mass(minMt), electron transverse momentum($p_T(e)$) and muon transverse momentum($p_T(\mu)$) distributions at preselection stage with m$_H=$ 145 GeV for the electron muon final state. The sharp rise of the rightmost bins are due to overflow.

V. FINAL SELECTION

The boosted decision tree (BDT) discriminant is used to demove the dominant W+jet/γ and multi-jet backgrounds at the preselection level (BDTw). The BDTw was trained for each Higgs boson mass point considered separately. The output of the BDTw is a single number, which characterizes the event as background-like or signal-like.

The following list of input variables were used for the BDTw:

- electron p_T;

- muon p_T;

- invariant mass of the electron and the muon;

- azimuthal distance between the electron and the muon, $\Delta\phi_{e\mu}$;

- distance in η and ϕ space between the electron and the muon, $\Delta\mathcal{R}_{e\mu}$;

- the missing transverse energy $\not{E}_T$;

- the special missing transverse energy $\not{E}_T^{\mathrm{special}}$, which is defined to reduce the impact of mis-measurement on $\not{E}_T$;

- minimum of transverse mass between $\not{E}_T$ and each lepton, $M_T^{\min}$;

- M_{T2}, a function of the momenta of two invisible particles and the missing transverse momentum in an event [17];

- the transverse momentum of the electron muon system;

- charged η ($q \times \eta$) of the electron

- charged η ($q \times \eta$) of the muon

- minimum of azimuthal angle between $\not{E}_T$ and each lepton;

- maximum of azimuthal angle between $\not{E}_T$ and each lepton;

- transverse mass between $\not{E}_T$ and dilepton pair, $M_T(\ell\ell, \not{E}_T)$;

- the Likelihood of the electron

A BDTw> 0.3 requirement is placed to reject most of the multijet and a large fraction of the W+jet/γ background. The BDTw discriminant for a Higgs boson mass of 115 GeV and 145 GeV are shown in Figure 2. As shown in
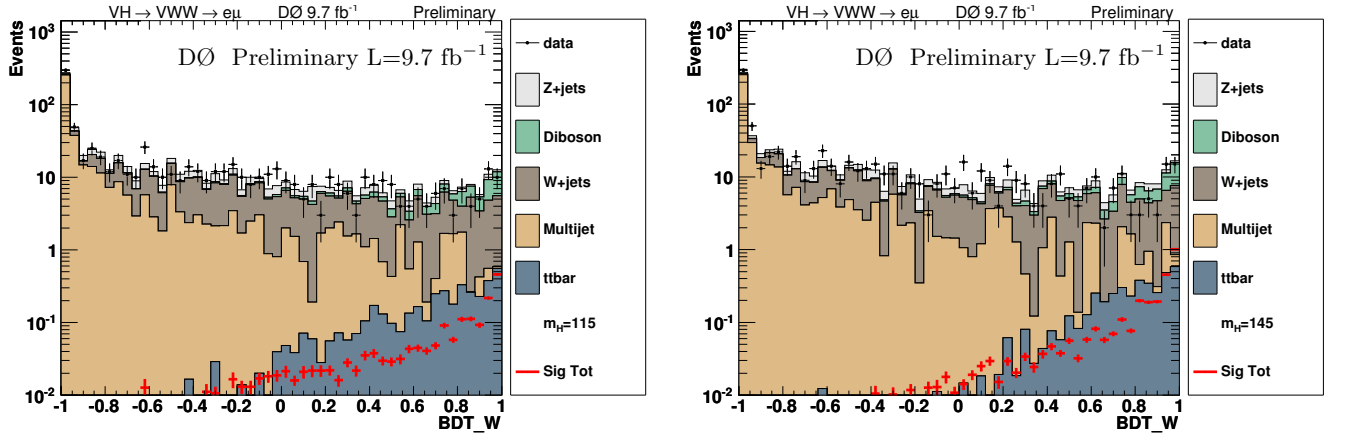

FIG. 2: The BDTw distribution at preselection stage with m_H= 115 GeV (left) and 145 GeV (right) for the electron muon final state.

Figure 1 in the minimum transverse mass (M_T^{min}) distribution, the very low bins are dominated by multijet events. To make sure the multijet events are reduced to minimum for the analysis, an additional criterion $M_T^{min} >7$ GeV is applied. The numbers of events at the final selection are shown in Table I, and the kinematic distributions are shown in Figure 3.
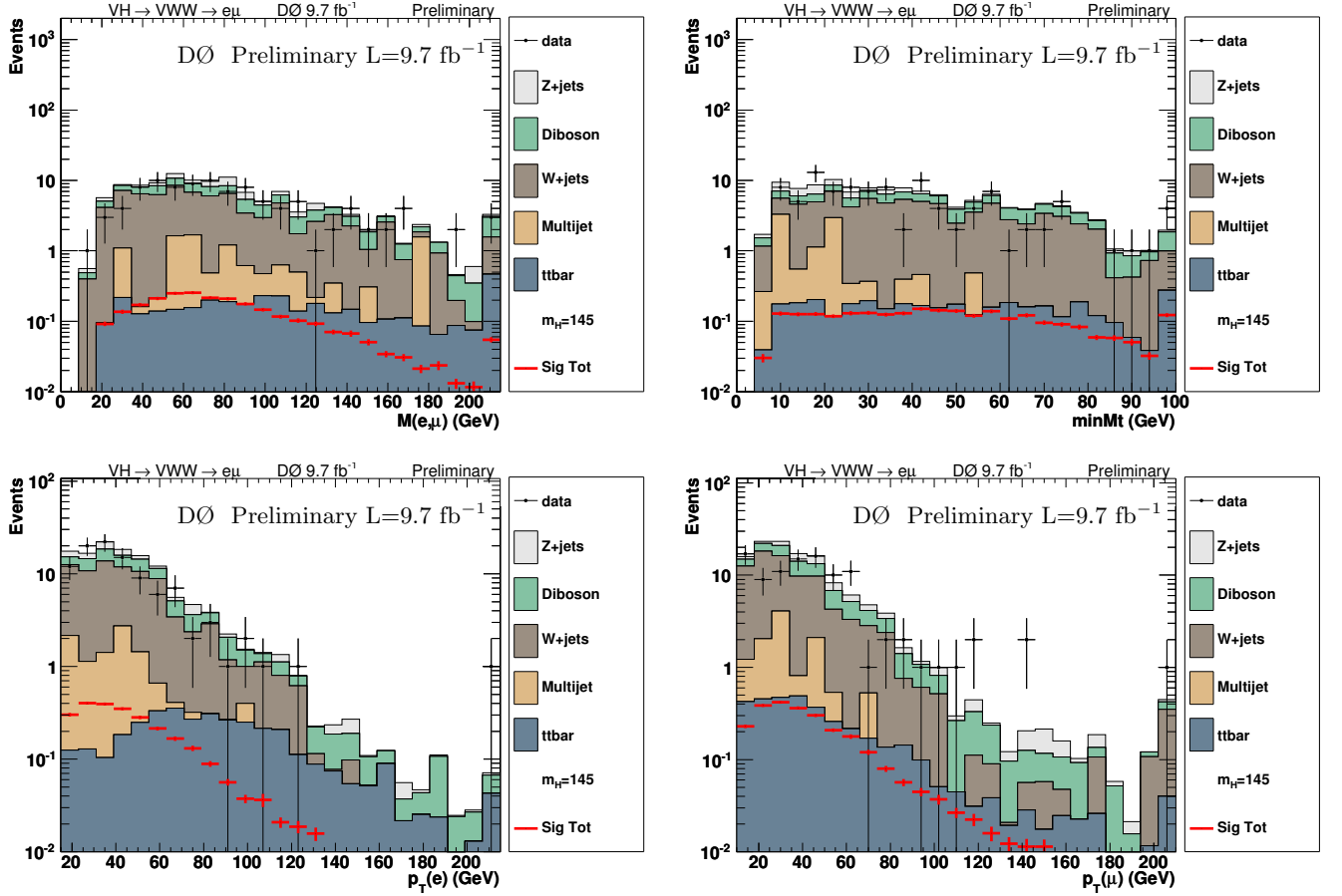
FIG. 3: The invariant mass(M(e,μ)), minimum transverse mass(minMt), electron transverse momentum($p_T(e)$) and muon transverse momentum($p_T(\mu)$) distributions after final selection with m_H= 145 GeV for the electron muon final state. The sharp rise of the rightmost bins are due to overflow.

VI. FINAL DISCRIMINANT

For the final selection, the signal is separated from the remaining background using an additional BDT. The final discriminant BDT (FD BDT) inputs includes all the variables used for the BDTw discriminant listed above with the addition of the following variables:

- Detector η of the electron, η^e.

- Detector η of the muon, η^μ.

- Number of jets.

Simulated events are used to train the BDT to differentiate between all Higgs boson signal events, and all background events for each Higgs boson mass considered. The BDT discriminant for Higgs boson mass of 115 GeV and 145 GeV are shown in Figure 4.

VII. RESULTS AND CONCLUSION

The analysis considers two types of systematics: systematics that affect normalization of the MC samples only and those affect differential distribution and therefore impact the shape of the FD BDT distributions.

Source of systematic uncertainties that affect normalization are: 6.2% for the VH signal production cross section calculation, 6% for the $t\bar{t}$ cross section calculation, 7% for the diboson cross section calculation, 4% for the normalization factor ($f_{normalization}$) dominated by the systematic uncertainty for the Z+jet cross section calculation which

Sample	Preselection	Final selection
Data	822	102
Signal	3.09	2.56
WH	2.65	2.21
ZH	0.44	0.35
Tot. bkg.	798.30	125.24
Z → ee	16.28	2.85
Z → $\mu\mu$	57.47	10.42
Z → $\tau\tau$	21.37	1.64
$t\bar{t}$	4.13	3.60
W+jet/γ	234.48	69.97
WW	3.56	2.69
WZ	28.23	22.53
ZZ	4.55	2.85
Multijets	428.23	8.69

TABLE I: Expected and observed number of events at preselection and after final selection in the like charge $e\mu$ final states. The signal assumes a Higgs boson mass of 145 GeV.
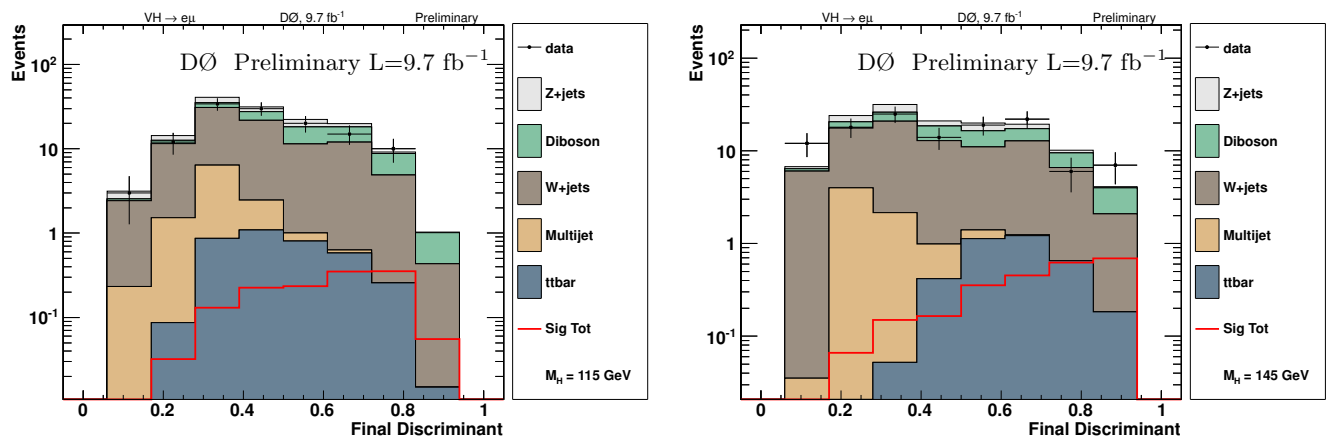
FIG. 4: The FD BDT distribution at final selection stage with m_H= 115 GeV (left) and 145 GeV (right) for the electron muon final state.

applied to all but Z+jet samples, 2% for the normalization uncertainty due to multijet estimation, 1.5% to account for any residual trigger biases, 50% on mis-modelling of the charge mismeasurement in the simulation in Z+jet and WW events.

The uncertainties that affect differential distributions of the W–p_T and W+jet/γ reweighting are determined by taking 50% of the difference of the results obtained with and without reweighting.

The observed FD BDT output distributions agree within uncertainties with the expected backgrounds as shown in Figure 4. The FD BDT output distributions are therefore used to set limits on the Higgs boson associated production cross section $\sigma(p\bar{p} \to VH)$ assuming SM values for the branching ratios and for the cross section of the associated Higgs boson production mechanisms considered. We calculate limits using a modified frequentist method (CLs), with a log-likelihood ratio (LLR) test statistic [18]. To minimize the degrading effects of systematics on the search sensitivity, the individual background contributions are fitted to the data observation by maximizing a profile likelihood function for the background-only and signal-plus-background hypotheses [19].

Table II presents expected and observed upper limits at 95% CL for $\sigma(p\bar{p} \to VH)$ relative to that expected in the SM for each Higgs boson mass considered. Figure 5 shows the expected and observed limits for $\sigma(p\bar{p} \to VH)$ relative to the SM for the different Higgs boson masses, while Figure 6 shows the corresponding LLR distribution. At $m_H = 145$ GeV, the observed limit ratio is 6.87, with 6.50 expected.

A search for the SM Higgs boson is presented in the final state with like charged electron muon pairs in $p\bar{p}$ collisions at a center-of-mass energy of $\sqrt{s} = 1.96$ TeV. The data analyzed corresponds to an integrated luminosity of $\mathcal{L} = 9.7$ fb^{-1}. Limits on the cross section of a Standard Model Higgs boson are presented.

Mass (GeV)	115	120	125	130	135	140	145	150	155	160	165	170	175	180	185	190	195	200
exp	15.78	12.67	11.58	9.22	7.85	7.41	6.50	6.00	6.72	6.13	5.89	7.27	7.46	7.76	8.64	10.42	11.23	11.06
obs	13.13	10.16	7.77	10.55	7.03	8.08	6.87	7.09	7.14	6.84	6.17	6.86	8.51	12.72	12.83	15.86	19.04	17.08

TABLE II: Expected and observed limits on $\sigma \times BR$ for Higgs boson masses between 115 and 200 GeV. The limits are given for the full Run II data.
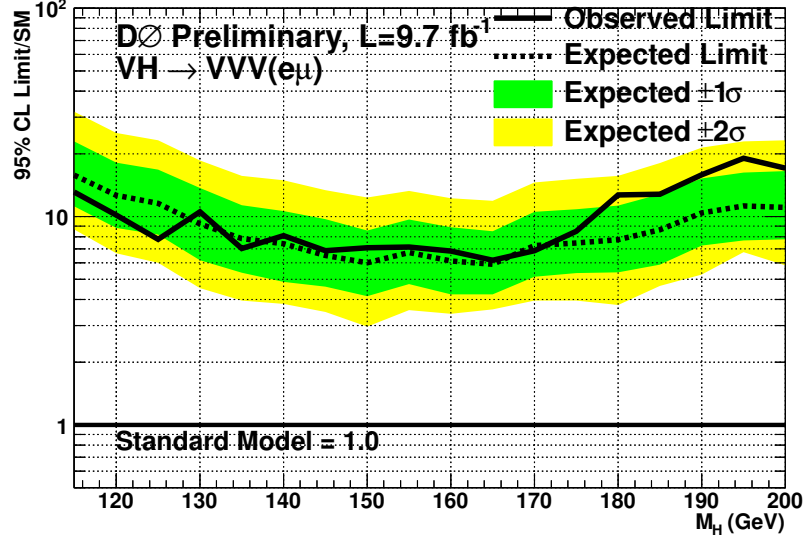
FIG. 5: Expected and observed limits at the 95% C.L. in units of the SM cross section as a function of M_H. The green and yellow shaded areas represent the $\pm 1\sigma$ and $\pm 2\sigma$ confidence bands. The dashed line represents the expected limit and the black line represents the observed limit.
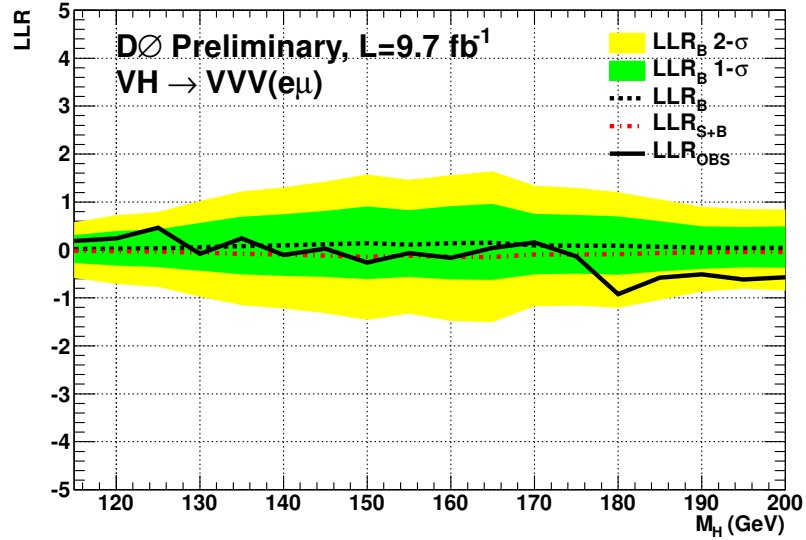

FIG. 6: The Log Likelihood Ratio(LLR) as a function of M_H for the Run 2 dataset. The black line represents the observed LLR. The green and yellow shaded areas represent the $\pm 1\sigma$ and $\pm 2\sigma$ confidence bands. The 'background-only' and 'background + signal' hypotheses are given by the black and red dashed lines respectively.

Acknowledgments

[1] DØ Collaboration, V. M. Abazov *et al.* Phys. Rev. D **84**, 092002 (2011).

[2] DØ Collaboration, V. M. Abazov *et al.*, Nucl. Instrum. Methods Phys. Res. A. **565**, 463 (2006).

[3] R. Angstadt et al Nucl. Instrum. Methods Phys. Res. A **622**, 298 (2010).

[4] M. Abolins et al, Nucl. Instrum. Methods Phys. Res. A **584**, 75 (2008).

[5] T. Sjöstrand *et al.*, Comp. Phys. Comm. **135**, 238 (2001), we use version 6.323 or later.

[6] The Tevatron New Phenomena and Higgs Working Group, FERMILAB, CDF Note 10474, `http://www-d0.fnal.gov/Run2Physics/higgs/xsbr/xsbr_Jan19_2012.pdf`.

[7] A. Djouadi, J. Kalinowski, and M. Spira, Comput. Phys. Commun. **108**, 56 (1998).

[8] M.L. Mangano, F. Piccinini, , A. D. Polosa, M. Moretti and R. Pittau, J. High Energy Phys. 07 (2003) 001, we use version 2.11.

[9] R. Hamberg, W.L. van Neerven, and T. Matsuura, Nucl. Phys. B**359**, 343 (1991) [Erratum-ibid. B**644**, 403 (2002)].

[10] J. Pumplin et al., J. High Energy Phys. 07 (2002) 012.

[11] DØ Collaboration, V. M. Abazov *et al.*, Phys. Rev. Lett. **100**, 102002 (2008)

[12] K. Melnikov and F. Petriello, Phys. Rev. D**74**, 114017 (2006).

[13] U. Langenfeld, S. Moch and P. Uwer, Phys. Rev. D**80**, 054009 (2009).

[14] J. M. Campbell, R. K. Ellis, `http://mcfm.fnal.gov/`.

[15] J. M. Campbell and R. K. Ellis, Phys. Rev. D**60**, 113006 (1999).

[16] G. C. Blazey *et al.*, [hep-ex/0005012] (2000)

[17] C. Lester and D. Summers, Phys. Lett. B **463**, 99-103 (1999).

[18] T. Junk, Nucl. Instrum. Methods Phys. Res. A. **434**, 435 (1999). A. Read, J. Phys. G **28** (2002) 2693-704.

[19] W. Fisher, FERMILAB-TM-2386-E.